J Nanopart Res (2017) 19: 285
DOI 10.1007/s11051-017-3985-5

RESEARCH PAPER

Synthesis and microstructure of Co/Ni: $MgGa_2O_4$ nanoparticles

Nannan Li · Jian Liu · Xiulan Duan · Fapeng Yu · Huaidong Jiang

Received: 9 January 2017 / Accepted: 26 July 2017 / Published online: 10 August 2017

Abstract This report discusses the preparation and microstructure of Co/Ni co-doped $MgGa_2O_4$ nanoparticles. The nanoparticles with the size of 20–55 nm were synthesized by sol-gel method. The phase and crystallinity were confirmed by X-ray powder diffraction (XRD) pattern. The particle size was estimated according to XRD data and transmission electron microscopy. The electronic structure was studied using X-ray photoelectron spectroscopy (XPS). The XPS studies showed that Ga^{3+} ions possess tetrahedral and octahedral sites of spinel structure and the inverse degree (two times of the fraction of tetrahedral Ga^{3+} ions) has increased with the increase of the doping concentration of Co^{2+} and Ni^{2+} ions. For Co/Ni co-doped $MgGa_2O_4$, two broad absorption bands of 350~500 and 550~700 nm were observed in the absorption spectra. The broad band at 350~500 nm was assigned to the combination of the absorption of octahedral Co^{2+} and Ni^{2+} ions, whereas the absorption band at 550~700 nm is mainly due to tetrahedrally coordinated Co^{2+} ions and octahedrally coordinated Ni^{2+} ions.

Keywords Sol-gel method · X-ray photoelectron spectroscopy · Electronic structure · Optical properties · Nanostructure

N. Li · J. Liu · X. Duan (✉) · F. Yu · H. Jiang
State Key Laboratory of Crystal Materials, Institute of Crystal Materials, Shandong University, Jinan 250100, People's Republic of China
e-mail: xlduan@sdu.edu.cn

Introduction

Magnesium gallate ($MgGa_2O_4$) is an electroluminescent material and has highly been attracted for applications in vacuum fluorescent and field emission displays (Costa et al. 2009; Moon et al. 2008; Pedro et al. 2015) because of its good chemical stability, low excitation voltage, and high purity of luminescence (Liu et al. 2013; Choi et al. 2010). It belongs to AB_2O_4 spinel-type oxides, where A and B are divalent and trivalent metal cations, respectively. The oxygen ions in AB_2O_4 arrange in close-packed cubic structure, forming tetrahedral and octahedral vacancies which are occupied by A and B cations. $MgGa_2O_4$ is known to be mixed spinel structure (Jiang et al. 2012; da Silva et al. 2013). The distribution of these cations in tetrahedral and octahedral sites classifies the spinel-type oxide material (AB_2O_4) into three types: (I) normal spinel: A and B ions occupy the tetrahedral and octahedral sites, respectively; (II) inverse spinel: a half of B ions occupy the tetrahedral position and the other half of B and all of A ions occupy the octahedral position; and (III) mixed spinel: A and B ions occupy the two different sites randomly. The distribution of A and B cations can be controlled by different preparation methods, type of impurities, and its concentration that will affect the material color, absorption, and emission properties (Liu et al. 2015; Yu et al. 2002; Kumar et al. 2004; Tsai et al. 2004).

Recently, $MgGa_2O_4$ doped with transition metal ions has attracted much attention because of strong emission and absorption properties in the visible region (Song et al. 2014; da Silva et al. 2010; Li et al. 2009; Yu and Liu

2011; Sun et al. 2016; Lv et al. 2009; Costa et al. 2012). The introduction of transition metal ions can tune the optical properties of spinel oxide materials. For example, Co- and Ni-doped $MgGa_2O_4$ materials show emissions at 685 nm (red) and 590 nm, respectively. At present, much work has been reported about the luminescence properties of $MgGa_2O_4$ doped with single active ions such as Cr^{3+}, Mn^{2+}, Ni^{2+}, Eu^{3+}, and Pr^{3+} (Pedro et al. 2015; Lv et al. 2009; Costa et al. 2012; Suzuki et al. 2008; Suzuki et al. 2005; Lv et al. 2010). Though many reports on optical properties, electronic structure of $MgGa_2O_4$ nanoparticles has seldom been studied (Yu et al. 2002; Kumar et al. 2004). To the best of our knowledge, the co-doping of Co and Ni in $MgGa_2O_4$ nanoparticle has not been reported. In this work, Co/Ni co-doped $MgGa_2O_4$ nanoparticles have been synthesized by the sol-gel method and the microstructure were probed through different analytical methods such as X-ray powder diffraction, TEM, and X-ray photoelectron spectroscopy (XPS). The influence of co-doping of transition elements (Co^{2+} and Ni^{2+}) on the structure and optical properties were discussed.

Experimental

Polycrystalline Co/Ni co-doped $MgGa_2O_4$ nanoparticles were prepared by citric acid-assisted sol-gel method. $Co(CH_3COO)_2{\cdot}4H_2O$ (AR, Shanghai Hengxin Chemical Reagent Factory), $Ni(NO_3)_2{\cdot}6H_2O$ (AR, Aladdin Chemistry Co.), $Mg(NO_3)_2{\cdot}6H_2O$ (AR, Tianjin Kermel Chemical Reagent Center), and $Ga(NO_3)_3{\cdot}xH_2O$ (AR, Aladdin Chemistry Co.) were used as starting materials. Calculated amount of these raw materials were dissolved in deionized water. Co and Ni concentrations (mol%) were varied to produce a range of $Co_xNi_yMg_{1-x-y}Ga_2O_4$ ($0.05 \le x \le 0.3$, $0.01 \le y \le 0.3$) stoichiometries. Citric acid was added into the above solution as a chelating agent. The molar ratio of metal ions to citric acid was 1:2; the pH of the solution was 3.0. The final solution was stirred for 1 h using a magnetic stirrer and then heated until formation of highly viscous gels. The gels were dried in an oven at 150 °C for 8 h followed by calcination at 800 °C for 5 h. The obtained nanoparticles were used for all the characterization studies.

Powder X-ray diffraction (XRD) data of the doped $MgGa_2O_4$ nanoparticles were collected on a Rigaku D/Max-rA diffractometer using a Cu Kα radiation (λ = 0.15418 nm) and with a graphite monochromator. The samples were step scanned in steps of 0.02° (2θ) using a count time of 0.1 s/step. Transmission electron micrographs were recorded using a JEM-2100 microscope. The samples were ultrasonicated in ethanol and then, a droplet of the suspension was deposited and dried on the sample support. The X-ray photoelectron spectra (XPS) were measured using a Thermofisher ESCALAB 250 spectrometer with monochromatized Al Kα radiation under ultrahigh vacuum (< 10^{-7} Pa). The binding energies were calibrated using C1s peak (284.6 eV) as a reference. All the peaks were deconvoluted after background subtraction using a mixed Gaussian–Lorentzian function. Diffuse absorbance spectra were recorded on a Shimadzu UV-2550 spectrophotometer with a step of 1 nm using an integration sphere at room temperature. $BaSO_4$ was used as reference.

Results and discussion

Synthesis of nanocrystals

The XRD patterns of the $Co_xNi_yMg_{1-x-y}Ga_2O_4$ nanoparticles annealed at 800 °C are presented in Fig. 1. The peaks indexed as (220), (311), (222), (400), (422), (511), and (440) crystal planes in the XRD patterns are assigned to cubic $MgGa_2O_4$ spinel phase (JCPDS No. 10-113). The intensity of the diffraction peaks increased, and the full width at half-maximum (FWHM) decreased with the increase of Co and Ni concentrations, which indicates the improved crystallinity. It can be seen that a weak diffraction peak due to MgO impurity phase (marked as "*" in

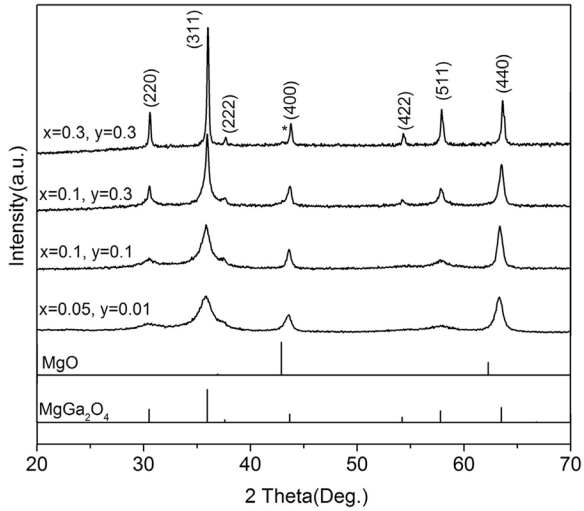

Fig. 1 XRD patterns of the $Co_xNi_yMg_{1-x-y}Ga_2O_4$ nanoparticles annealed at 800 °C

Table 1 Particle size of $Co_xNi_yMg_{1-x-y}Ga_2O_4$ nanoparticles obtained from XRD and TEM

Composition (x, y)	Particle size (nm)	
	XRD	TEM
0.05, 0.01	13	15
0.1, 0.1	16	20
0.1, 0.3	22	25
0.3, 0.3	50	55

Fig. 1) appeared when x = 0.1 and y = 0.3, and the intensity of the diffraction peak of MgO impurity increased with the increase of Co and Ni concentrations.

The average particle size of the samples was calculated by means of the Scherrer formula $D = 0.9\lambda/(\beta\cos\theta)$, where λ is the X-ray wavelength (0.15418 nm), β is the FWHM, and θ is the diffraction angle of the high intense peak. The size of the Co/Ni-doped $MgGa_2O_4$ nanoparticle is about 13 nm when $x = 0.05$ and $y = 0.01$, and the size increases to 50 nm when $x = 0.3$ and $y = 0.3$ (Table 1). The particle size increases dramatically when Ni content increases from 0.1 to 0.3. It may be that the doped Ni^{2+} ions occupy the position of Ga^{3+} ions, and the ionic radius of Ni^{2+} (69 pm) is larger than that of Ga^{3+} (62 pm), which makes the size of the particle increase.

The TEM images of the $Co_xNi_yMg_{1-x-y}Ga_2O_4$ nanoparticles are shown in Fig. 2. It can be seen from the figure that the particle shape is not regular. The particle size is in the range 15~55 nm and the size increases with the increase of dopant concentration. The TEM results are consistent with those of XRD (Table 1).

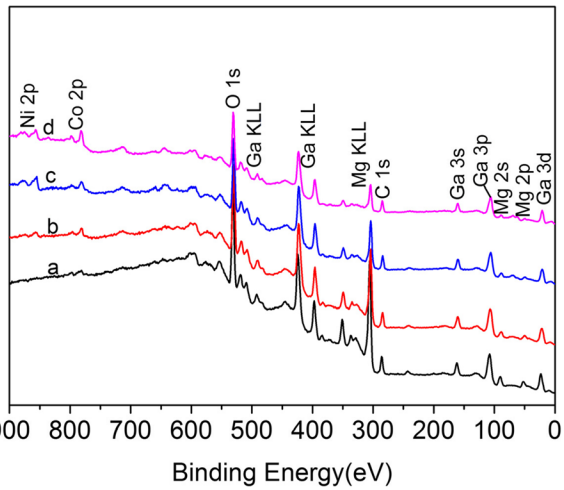

Fig. 3 XPS survey spectra of $Co_xNi_yMg_{1-x-y}Ga_2O_4$ nanoparticles annealed at 800 °C: (*a*) $x = 0.05$, $y = 0.01$; (*b*) $x = 0.1$, $y = 0.1$; (*c*) $x = 0.1$, $y = 0.3$; (*d*) 0.3, 0.3

Electronic structure

The composition and the electronic structure of as-prepared Co/Ni co-doped $MgGa_2O_4$ nanoparticles were

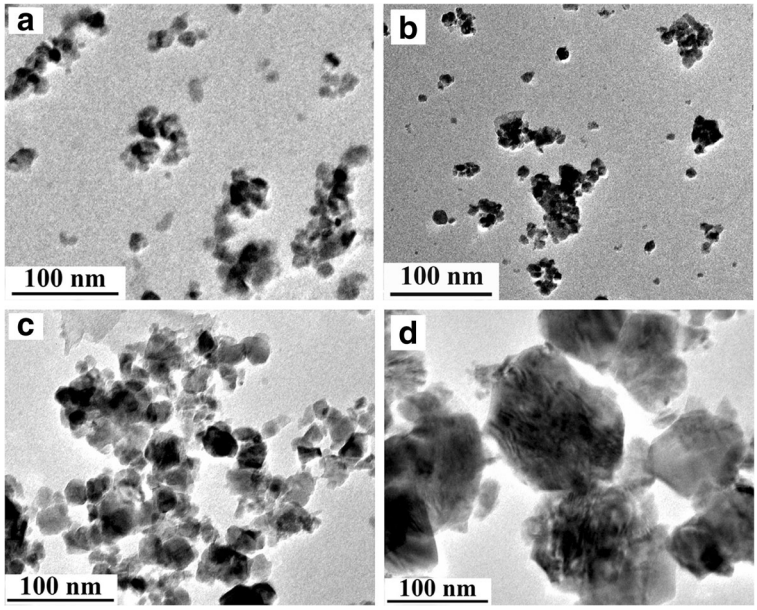

Fig. 2 TEM images of $Co_xNi_yMg_{1-x-y}Ga_2O_4$ nanoparticles annealed at 800 °C: **a** $x = 0.05$, $y = 0.01$; **b** $x = 0.1$, $y = 0.1$; **c** $x = 0.1$, $y = 0.3$; **d** $x = 0.3$, $y = 0.3$

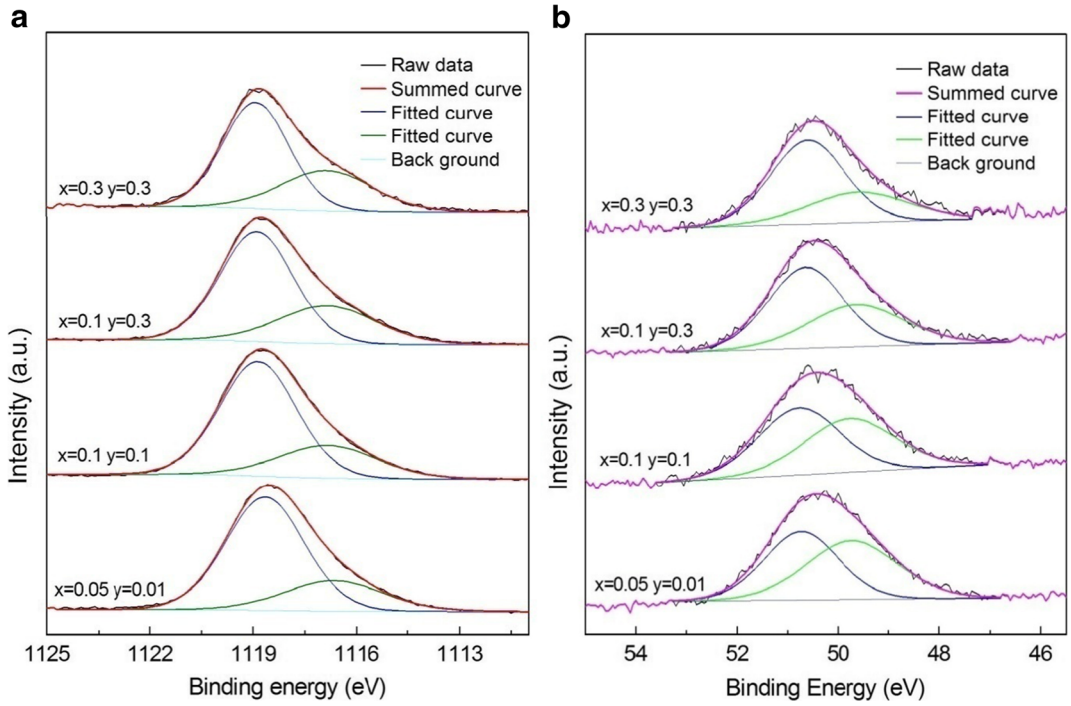

Fig. 4 XPS core level spectra of $Co_xNi_yMg_{1-x-y}Ga_2O_4$ nanoparticles annealed at 800 °C: **a** Ga $2p_{3/2}$; **b** Mg 2p

determined through XPS analysis. Figure 3 shows the XPS survey spectra of the $Co_xNi_yMg_{1-x-y}Ga_2O_4$ nanoparticles. The XPS core level spectra of Ga 2p, Mg 2p, Co 2p, and Ni 2p were collected as shown in Figs. 4 and 5. The XPS survey spectra revealed that no other elements were detected except contaminated carbon. The C 1s peak at 284.6 eV were used for calibration.

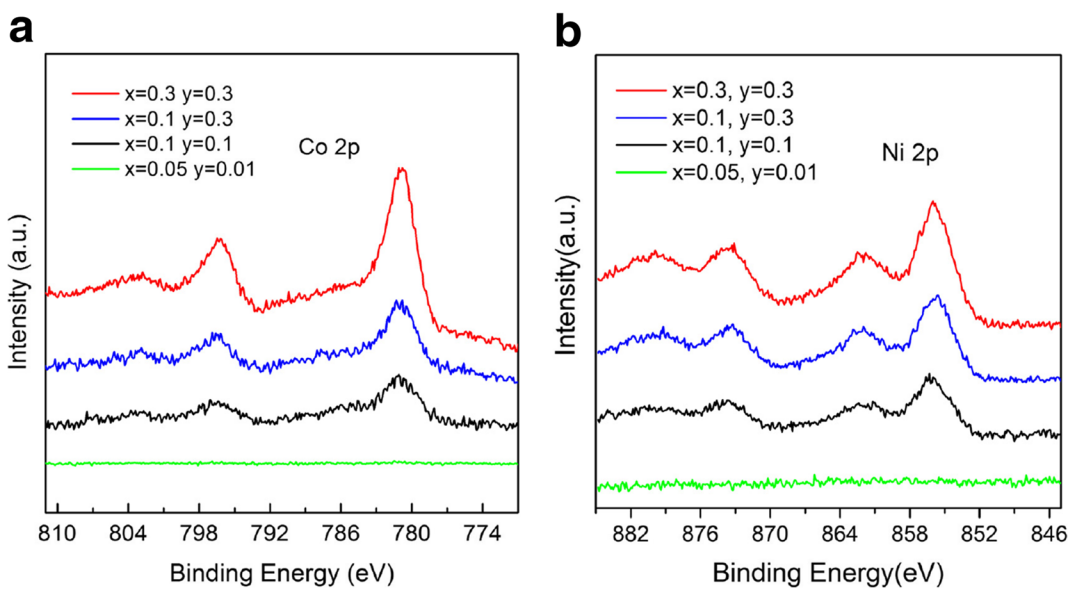

Fig. 5 XPS core level spectra of $Co_xNi_yMg_{1-x-y}Ga_2O_4$ nanoparticles annealed at 800 °C: **a** Co 2p; **b** Ni 2p

Table 2 XPS data for Ga $2p_{3/2}$ spectra of $Co_xNi_yMg_{1-x-y}Ga_2O_4$ nanoparticles annealed at 800 °C

Composition (x, y)	Binding energy (± 0.1 eV)	Area percent (± 0.5%)	FWHM (± 0.1 eV)	Fraction of tetrahedral Ga^{3+}
0.05, 0.01	1118.6	74.7	2.8	0.25
	1116.6	25.3	3.5	
0.1, 0.1	1118.8	73.0	2.7	0.27
	1116.8	27.0	3.5	
0.1, 0.3	1118.9	68.5	2.6	0.31
	1116.8	31.5	3.5	
0.3, 0.3	1118.9	65.4	2.4	0.35
	1116.8	34.6	3.2	

Figure 4a shows the Ga $2p_{3/2}$ spectra of $MgGa_2O_4$ nanoparticles with different concentrations of Co and Ni dopants. It can be found that all the spectra are asymmetric, indicating more than one chemical state of Ga^{3+} ions. After deconvolution, Ga $2p_{3/2}$ spectra are divided into two peaks, indicating the Ga^{3+} ions occupy two different coordination sites. The compositional details and peak parameters of Ga^{3+} are listed in Table 2. The peaks located at 1118.8 eV and 1116.8 eV are respectively assigned to octahedral and tetrahedral Ga^{3+} ions. When $x = 0.05$ and $y = 0.01$, the inversion degree (two times of the fraction of tetrahedral Ga^{3+} ion) is 0.5, and the value increases with the increase of the doping concentration. When both x and y are equal to 0.3, the inversion parameter is increased to 0.70.

The Mg 2p XPS spectra (Fig. 4b) are also not symmetric and consist of two peaks. The peak at 50.6 eV can be assigned to Mg^{2+} ion in octahedral site, and the peak at 49.7 eV can be ascribed to Mg^{2+} ion in tetrahedral site. These values are consistent with the literature reports (Ono et al. 2001; Zakaznova-Herzog et al. 2006). The fraction of octahedral Mg^{2+} ion is 0.48 when $x = 0.05$ and $y = 0.01$, and this value increases to 0.67 when $x = 0.3$ and $y = 0.3$. The compositional details and peak parameters of Mg^{2+} are listed in Table 3.

Table 3 XPS data for Mg 2p spectra of $Co_xNi_yMg_{1-x-y}Ga_2O_4$ nanoparticles annealed at 800 °C

Composition (x, y)	Binding energy (± 0.1 eV)	Area percent (± 0.5%)	FWHM (± 0.1 eV)	Fraction of octahedral Mg^{2+}
0.05, 0.01	50.7	48.4	1.8	0.48
	49.7	51.6	2.2	
0.1, 0.1	50.7	52.6	1.9	0.53
	49.7	47.4	2.2	
0.1, 0.3	50.6	60.3	1.8	0.60
	49.6	39.7	2.3	
0.3, 0.3	50.6	66.7	1.8	0.67
	49.6	33.3	2.4	

Figure 5a shows the Co 2p XPS spectra of $Co_xNi_yMg_{1-x-y}Ga_2O_4$ nanoparticles with different concentrations of Co and Ni dopants. The peak around 781 eV is ascribed to high-spin nature of divalent cobalt, and this value is consistent with Co^{2+} in other materials (Stelmachowski et al. 2014; Sharma et al. 2008). The FWHM is relatively wide probably because of the Co^{2+} ions occupy two different sites in the nanoparticles. The Ni 2p XPS spectra are displayed in Fig. 5b. The peak at 855.4 eV associated with the satellite peak at 861.6 eV is assigned to Ni $2p_{3/2}$, which is consistent with the literatures (Zhang et al. 2009; Bennet et al. 2016; Mittal et al. 2006). The compositional details and peak parameters of Co $2p_{3/2}$ and Ni $2p_{3/2}$ are listed in Table 4.

Optical properties

To study the relationship between the structure and optical properties of $Co_xNi_yMg_{1-x-y}Ga_2O_4$ nanoparticles, the absorption spectra were recorded as presented in Fig. 6. The Ni-doped $MgGa_2O_4$ shows two absorption peaks at 370 and 650 nm; this can be assigned to the transition of $^3A_{2g}(^3F) \rightarrow {}^3T_{1g}(^3P)$ and $^3A_{2g}(^3F) \rightarrow {}^3T_{1g}(^3F)$ of Ni^{2+} in the octahedral sites, respectively (Suzuki

Table 4 Binding energies of Co $2p_{3/2}$ and Ni $2p_{3/2}$ core levels (eV) of $Co_xNi_yMg_{1-x-y}Ga_2O_4$ nanoparticles annealed at 800 °C

Composition (x, y)	Co $2p_{3/2}$ (± 0.1 eV)	Ni $2p_{3/2}$ (± 0.1 eV)
0.1, 0.1	781.0	855.4
0.1, 0.3	780.9	855.2
0.3, 0.3	780.8	855.1

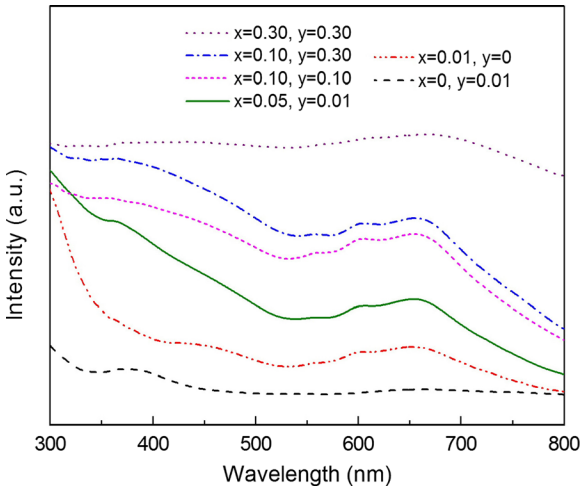

Fig. 6 Absorption spectra of $Co_xNi_yMg_{1-x-y}Ga_2O_4$ nanoparticles with different doping concentrations

et al. 2008; Suzuki et al. 2010). Similarly, for Co-doped sample, two broad bands at around 400~500 and 550~700 nm were observed. The absorption band at 400~500 nm is assigned to Co^{2+} ions in octahedral sites, and the absorption peaks at 550, 600, and 650 nm are assigned to the spin-allowed of $^4A_2$ (^4F) → $^2T_2$ (^2G), $^4A_2$ (^4F) → $^2T_1$ (^2G), and $^4A_2$ (^4F) → $^4T_1$ (^4P) transition of Co^{2+} in tetrahedral sites, respectively (Chen et al. 2002; Gaudon et al. 2009). For Co/Ni co-doped $MgGa_2O_4$, the broad band at 350~500 nm is the combination of the absorption of octahedral Co^{2+} and Ni^{2+} ions, while the band at 550~700 nm is mainly due to tetrahedral Co^{2+} and octahedral Ni^{2+} ions. The absorption intensity of the peaks increases with increasing concentration of Co^{2+} and Ni^{2+} ions.

Conclusion

$Co_xNi_yMg_{1-x-y}Ga_2O_4$ nanoparticles with the size of 15~55 nm were synthesized by citric acid-assisted sol-gel method. The powder XRD pattern confirmed the synthesized $MgGa_2O_4$ phase and particles size were increased with increase of dopant concentrations. The XPS spectra indicate that Ga^{3+} and Mg^{2+} ions occupy both the tetrahedral and octahedral sites. The fraction of tetrahedral Ga^{3+} ions increases with increasing doping concentration, which is consistent with the change of the proportion of octahedral Mg^{2+} ions. The inverse parameter increases with the increase of the doping concentrations. Two broad absorption bands at 350~500 and 550~700 nm were observed for Co/Ni co-doped $MgGa_2O_4$. The absorption is attributed to the combination of octahedral or tetrahedral Co^{2+} and octahedral Ni^{2+} ions. The intensity of the absorption bands increases with the increase of dopant concentrations of Co and Ni.

Acknowledgements This work was supported by grants from the National Natural Science Foundation of China (Nos. 51172130 and 51672160).

Compliance with ethical standards

Conflict of interest statement The authors declare that they have no conflict of interest.

References

Bennet J, Tholkappiyan R, Vishista K, Victor Jaya N, Hamed F (2016) Attestation in self-propagating combustion approach of spinel AFe_2O_4 (A = Co, Mg and Mn) complexes bearing mixed oxidation states: magnetostructural properties. Appl Surf Sci 383:113–125

Chen ZZ, Shi EW, Li WJ, Zheng YQ, Zhong WZ (2002) Hydrothermal synthesis and optical property of nano-sized $CoAl_2O_4$ pigment. Mater Lett 55:281–284

Choi S, Kim K, Moon YM, Park BY, Jung HK (2010) Rapid synthesis of spherical-shaped green-emitting $MgGa_2O_4$: Mn^{2+} phosphor via spray pyrolysis. Mater Res Bull 45: 979–981

Costa GKB, Pedro SS, Carvalho ICS, Sosman LP (2009) Preparation, structure analysis and photoluminescence properties of $MgGa_2O_4$: Mn^{2+}. Opt Mater 31:1620–1627

Costa GKB, Sosman LP, Lopez A, Cella N, Barthem RB (2012) Optical and structural properties of Ni^{2+}-doped magnesium gallate polycrystalline samples. J Alloys Compd 534:110–114

da Silva MAFM, da Silva Pedro S, Sosman LP (2010) Cr^{3+} impurity concentration and excitation dependences of magnesium gallate spinel photoluminescent data. J Alloys Compd 492:282–285

da Silva MAFM, Carvalho ICS, Cella N, Bordallo HN, Sosman LP (2013) Evidence of broad emission band in the system $MgGa_2O_4$–Ga_2O_3 doped with Cr^{3+} ions. Opt Mater 35:543–546

Gaudon M, Apheceixborde A, Menetrier M, Le Nestour A, Demourgues A (2009) Synthesis temperature effect on the structural features and optical absorption of $Zn_{1-x}Co_xAl_2O_4$ oxides. Inorg Chem 48:9085–9091

Jiang C, Sickafus KE, Stanek CR, Rudin SP, Uberuaga BP (2012) Cation disorder in MgX_2O_4 (X = Al, Ga, In) spinels from first principles. Phys Rev B 86:024203

Kumar VR, Narasimhulu KV, Gopal NO, Jung HK, Chakradhar RPS, Rao JL (2004) EPR, luminescence and IR studies of

Mn activated $ZnGa_2O_4$ phosphor. J Phys Chem Solids 65: 1367–1372

Li YX, Niu PJ, Hu L, Xu XW, Tang CC (2009) Monochromatic blue-green and red emission of rare-earth ions in $MgGa_2O_4$ spinel. J Lumin 129:1204–1206

Liu H, Yu LX, Li FH (2013) Photoluminescent properties of Eu^{3+} and Dy^{3+} ions doped $MgGa_2O_4$ phosphors. J Phys Chem Solids 74:196–199

Liu J, Duan XL, Li NN, Jiang HD (2015) Effects of synthesis method on cation distribution and optical properties of Co/Cr co-doped $MgGa_2O_4$ nanoparticles. J Alloys Compd 640: 169–174

Lv HL, Du JY, Tang ZQ, Liu CN (2009) Nanocrystals of Co^{2+}-doped $MgGa_2O_4$: preparation by a low-temperature combustion method and optical properties. J Chin Chem Soc 56: 323–326

Lv HL, Du JY, Ma Y, Ma WL, Liu JQ (2010) Synthesis and characterization of $Zn_xMg_{1-x}Ga_2O_4$: Co^{2+} fabricated by low-temperature burning method. Powder Technol 203: 428–431

Mittal VK, Chandramohan P, Bera S, Srinivasan MP, Velmurugan S, Narasimhan SV (2006) Cation distribution in $Ni_xMg_{1-x}Fe_2O_4$ studied by XPS and Mossbauer spectroscopy. Solid State Commun 137:6–10

Moon YM, Choi S, Jung HK, Lim SH (2008) Sensitized photoluminescent properties of manganese-activated magnesium gallate phosphor. J Lumin 128:1491–1495

Ono S, Asami K, Masuko N (2001) Mechanism of chemical conversion coating film growth on magnesium and magnesium alloys. Mater Trans 42:1225–1231

Pedro SS, Dasilva MAFM, Lopez A, Sosman LP (2015) Structural and photoluminescent properties of the $MgGa_2O_4$: Co^{2+} ceramic compound revisited after two decades. J Adv Ceram 4: 267–271

Sharma Y, Sharma N, Rao GVS, Chowdari BVR (2008) Studies on spinel cobaltites, $FeCo_2O_4$ and $MgCo_2O_4$ as anodes for Li-ion batteries. Solid State Ionics 179:587–597

Song EH, Wang JL, Yu DC, Ye S, Zhang QY (2014) Anomalous tunable visible to near infrared emission in the Mn^{2+}-doped spinel $MgGa_2O_4$ and room-temperature upconversion in the Mn^{2+} and Yb^{3+} co-doped spinel. J Mater Chem C 2:8811–8816

Stelmachowski P, Maniak G, Kaczmarczyk J, Zasada F, Piskorz W, Kotarba A, Sojka Z (2014) Mg and Al substituted cobalt spinels as catalysts for low temperature deN_2O—evidence for octahedral cobalt active sites. Appl Catal B Environ 146: 105–111

Sun JJ, Yu LX, Li FH, Wei SL, Li SC (2016) Up-conversion and near infrared luminescence in Er^{3+}/Yb^{3+} co-doped glass-ceramic containing $MgGa_2O_4$ nanocrystals. J Lumin 170:444–450

Suzuki T, Murugan GS, Ohishi Y (2005) Spectroscopic properties of a novel near-infrared tunable laser material Ni: $MgGa_2O_4$. J Lumin 113:265–270

Suzuki T, Arai Y, Ohishi Y (2008) Quantum efficiencies of near-infrared emission from Ni^{2+}-doped glass-ceramics. J Lumin 128:603–609

Suzuki T, Hughes M, Ohishi Y (2010) Optical properties of Ni-doped $MgGa_2O_4$ single crystals grown by floating zone method. J Lumin 130:121–126

Tsai BS, Chang YH, Chen YC (2004) Nanostructured red-emitting $MgGa_2O_4$: Eu^{3+} phosphors. J Mater Res 19:1504–1508

Yu LX, Liu H (2011) Photoluminescent properties of Dy^{3+} in MgO-Ga_2O_3-SiO_2 nano-glass-ceramic prepared by sol–gel method. Phys B 406:3101–3103

Yu M, Lin J, Zhou YH, Wang SB (2002) Citrate–gel synthesis and luminescent properties of $ZnGa_2O_4$ doped with Mn^{2+} and Eu^{3+}. Mater Lett 56:1007–1013

Zakaznova-Herzog VP, Nesbitt HW, Bancroft GM, Tse JS (2006) High resolution core and valence band XPS spectra of non-conductor pyroxenes. Surf Sci 600:3175–3186

Zhang L, Li F, Xiang X, Wei M, Evans DG (2009) Ni-based supported catalysts from layered double hydroxides: tunable microstructure and controlled property for the synthesis of carbon nanotubes. Chem Eng J 155:474–482